The calibration and use of n-hole velocity probes

Samantha Shaw-Ward*, Alex Titchmarsh, David M. Birch†
University of Surrey, Guildford, Surrey, UK GU2 7XH

A generalized calibration process is presented for multi-hole, pressure-based velocity probes which is independent of the number of holes and probe geometry, allowing the use of probes with large numbers of holes. The calibration algorithm is demonstrated at low speeds with a conventional seven-hole pressure probe and a novel nineteen-hole pressure probe. Because the calibration algorithm is independent of probe configuration, it is very tolerant of data corruption and imperfections in the probe tip geometry. The advantages of using probes with large numbers of holes is demonstrated in a conventional wing wake survey. The nineteen-hole probe offers a higher angular sensitivity than a conventional seven-hole probe, and can accurately measure velocity components even when an analytical calibration scheme is used. The probe can also provide local estimates of the diagonal components of the cross-flow velocity gradient tensor in highly vortical flows.

I. Introduction

Despite their comparative simplicity, multi-hole pressure probes continue to be used in the characterization of three-dimensional flows owing to their reliability, robustness and ease of manufacture. Furthermore, because they can provide local measurements of the three components of fluid velocity as well as of the local static and total pressure, they are of particular use in wake surveys (see [1, 2, 3, 4] and references cited therein), for which optical methods may present difficulties owing to the potential flow interference arising from particle injection [5] and particle momentum effects [6].

The design, calibration and use of five- and seven-hole probes is already well-developed (see, for example [7, 8, 9, 10, 11]). In general, the calibration process involves the identification of nondimensional pressure coefficients which are as sensitive as possible to the flow angularity but are insensitive to the velocity magnitude. These coefficients are then measured in steady flow over a range of incident flow angles during a calibration procedure; the range of angular sensitivity will depend on both the velocity magnitude and the probe tip geometry. Because the flow angularity has two degrees of freedom, at least two independent coefficients are required. Estimates of the local static and total pressure are also identified, and the errors between the estimates and actual

*Graduate Research Assistant, Department of Mechanical Engineering Sciences, Associate Member AIAA
†Lecturer, Department of Mechanical Engineering Sciences, Senior Member AIAA, d.birch@surrey.ac.uk

values (which are also a function of the flow angle) are similarly nondimensionalized and measured over a range of flow angles. The result of the calibration process is typically a set of four calibration functions mapping the nondimensionalized pitch angle, yaw angle, static pressure and total pressure to the pressures measured at the probe ports. These functions are generally either stored in the form of a look-up table (see [12]) or approximated as a polynomial expansion [9, 8]. A detailed comparison of these two calibration techniques is provided by Sumner [13].

Given any experimental measurement, then, the four coefficients are computed from the pressure readings, and the corresponding pitch angle, yaw angle, static pressure and total pressure are obtained either by interpolation or by functional approximation. The velocity magnitude may be determined from the static and total pressures, and the Cartesian velocity components may then be resolved. For probes with tips having well-defined geometries, it is also possible to obtain theoretical estimates of the four calibration functions based on either analytical or numerical solutions for the surface pressures; these techniques, however, are hindered by the high sensitivity of these idealized solutions to small manufacturing imperfections in the probe geometry, as well as by a loss of sensitivity in flows of very high vorticity [14].

More recently, a number of novel geometries and calibration algorithms have been proposed for probes having twelve and more holes, capable of resolving even reverse flow ([15, 16, 17]). The calibration technique proposed by Ramakrishnan & Rediniotis [15] is particularly attractive, as it is generalized and independent of both probe geometry and hole position; this method, however, still relies upon the identification and use of piecewise functions to represent the calibration surface. Calibration schemes such as that of Benay [18] are also of great value, as the procedure is generalized in the sense that it does not require the division of the probe measurement space into sectors, nor does it constrain the probe geometry.

The purpose of this work is to demonstrate the use of a continuous, generalized calibration scheme with probes having an arbitrary number of arbitrarily-arranged holes, and assess the robustness of the data reduction algorithm against some of those discussed above. In addition, the use of probes with large numbers of holes for the measurement of velocity components without calibration, as well as for the direct measurement of the local velocity gradients, is investigated.

II. Experimental setup

Experiments were carried out in an open-return wind tunnel with a working section of 0.9 m $\times$ 0.6 m. The free-stream velocity magnitude was set to $U_\infty = 10$ m/s for all of the measurements, and was maintained constant to within measurement precision by means of a closed-loop active control system. The control system sampled the average free-stream velocity averaged over 30-second intervals just upstream of the main measurement station, using a Pitot probe and a Furness micromanometer having a full-scale range of 196 Pa.

The directional velocity probes being tested were mounted in a five degree-of-freedom traverse

capable of translation in x, y and z (the streamwise, vertical and trasnverse axes, respectively) with a precision of ± 5 μm, and rotation in cone angle θ and roll ϕ with a precision of $\pm 0.2^\circ$ (where ϕ is a rotation about the x-axis). Probes were calibrated *in situ* over an angular range of $-60^\circ \leq \alpha \leq 60^\circ$ and $-60^\circ \leq \beta \leq 60^\circ$ (where α and β are the pitch and yaw angles of the probe axis, respectively). The probe measurement volume was not held stationary through the calibration process; however, scans carried out within the envelope of probe movement showed the variation in the freestream velocity was less than the overall measurement uncertainty.

The probes were connected via lengths of silicone tubing to an array of low-cost Honeywell PCAFA6D differential pressure sensors, referenced to the wind tunnel static pressure and driven by Burr-Brown INA125 bridge signal amplifiers to a net sensitivity of ~ 0.04 Pa/V. The analogue signals were routed through DG408 analogue signal multiplexers, and digitized using a Data Translation DT9836 data acquisition system. In all cases, a total of 10^4 samples were collected over 20 s, in order to ensure statistical convergence of the mean pressures. The pressure transducers were calibrated simultaneously against a micromanometer, by exposing the probe tip to quiescent air at controlled pressures. Transducer calibration was carried out before and after each experiment, and data were rejected if the calibration coefficients varied by more than 1%. The experimental setup and wind tunnel coordinate system are illustrated in Figure 1.

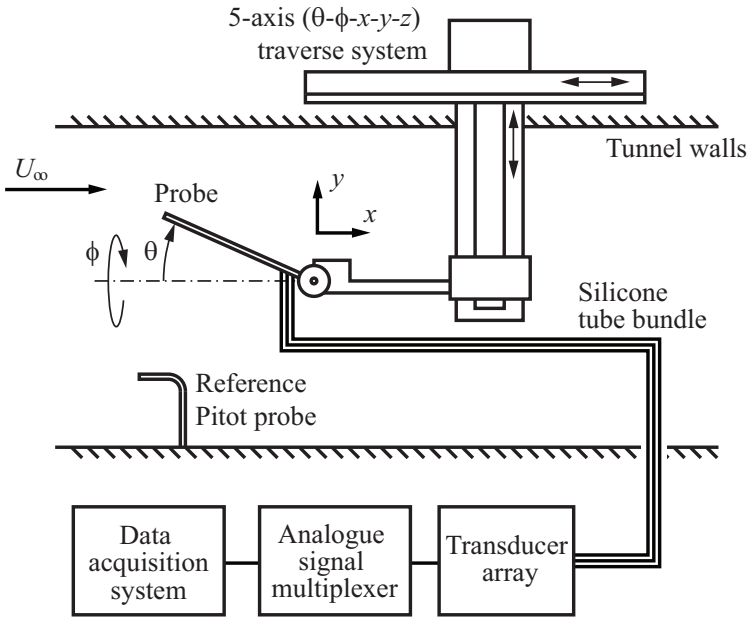

Figure 1. Schematic of experimental setup.

Two probes were constructed and tested. The first was a conventional miniature seven-hole probe, having a diameter of 2.5 ± 0.04 mm and an apex angle of 30°. The probe tip was precision-machined from solid brass; the holes were drilled to a nominal diameter of 0.5 mm, with a centre-to-centre spacing of 1.0 ± 0.06 mm. The second probe had nineteen holes, with seven central holes

in a closed-packed arrangement, surrounded by twelve peripheral holes arranged axisymetrically. The probe was constructed by assembling and soldering together lengths of 21-gauge stainless steel tubing, resulting in holes 0.51 ± 0.04 mm in diameter, with a centre-to-centre spacing of 0.81 ± 0.04 mm. The probe outer diameter was 4 ± 0.08 mm, and the probe tip was precision-machined after assembly to a hemispherical profile having a radius $R = 3.0 \pm 0.2$ mm. The configuration and hole index conventions for the seven- and nineteen-hole probes are shown in Figure 2.

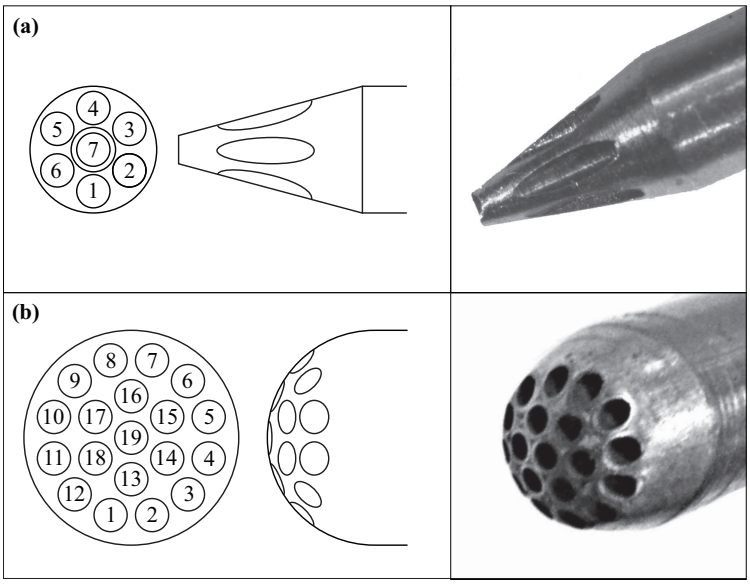

Figure 2. Schematic of probe geometries, including hole numbering conventions used and photographs of probe tips. (a) Conventional seven-hole probe; (b) nineteen-hole probe.

The probes were used to collect wake survey data behind a finite wing model, as wing tip vortices offer a velocity field which is strongly three-dimensional, highly vortical and easily validated as tip vortices tend to closely approximate a Batchelor vortex [19, 20]. The wing used had a uniform NACA 0012 profile with no taper or twist, and was fitted with a matching NACA 0012 body-of-revolution end-cap to minimize the generation of secondary vortices (see [21]). The wing had a chord $c = 157$ mm and an aspect ratio of 2.5, resulting in a chord Reynolds number $Re_c = U_\infty c/\nu \sim 1.05 \times 10^5$ (where ν is the kinematic viscosity). The wing was set at an angle of attack of ranging from 5° to 12° relative to the tunnel axis, and in all cases the wake surveys were collected at $x/c = 5$ downstream of the trailing edge, with the probe axis aligned with the free-stream flow.

III. Calibration algorithms

A. Conventional seven-hole probe calibration technique

As discussed above, there exist a number of different conventional techniques for the calibration of seven hole probes, and the definitions of the nondimensional coefficients will vary. Here, the

sectorized normalization technique of Wenger & Devenport [12] is adopted.

The seven-hole probe calibration process requires the assumption that the flow remains attached only in the immediate vicinity of the hole registering the maximum pressure. For small flow angles, then, the central hole will register the largest pressure. In this case, the pressures are converted into nondimensional coefficients as

$$\begin{aligned} C_\alpha &= \frac{P_4 - P_1}{P_7 - \overline{P}} \\ C_\beta &= \frac{P_5 + P_6 - P_2 - P_3}{2\left(P_7 - \overline{P}\right)}, \end{aligned} \tag{1}$$

where C_α and C_β are coefficients sensitive to the pitch yaw angle, respectively; $\overline{P}$ is defined here as

$$\overline{P} = \frac{1}{6}\sum_{k=1}^{6} P_k, \tag{2}$$

and the subscripts indicate the hole indices, defined as shown in Figure 2. In order to obtain local measurements of the velocity magnitude, approximations of the local static and stagnation pressures are also required. The stagnation pressure is approximated as the pressure at the central hole, and the static pressure is approximated as the mean pressure at the six peripheral holes; the difference $P_7 - \overline{P}$ therefore approximates the local dynamic pressure. The stagnation pressure coefficient C_0 and static pressure coefficient C_s are then defined as

$$\begin{aligned} C_0 &= \frac{P_7 - P_0}{P_7 - \overline{P}} \\ C_s &= \frac{\overline{P} - P_s}{P_7 - \overline{P}}, \end{aligned} \tag{3}$$

where P_0 and P_s are the true stagnation and static pressures measured in the free-stream flow (generally by an independent reference probe).

For flows of large angularity, the maximum pressure will be recorded at some hole i such that $i \neq 7$, and it may be assumed that the flow is attached only in the immediate vicinity of hole i. In this case, it becomes more convenient to express the flow angles in spherical coordinates; the different flow angles and velocity components are illustrated in Figure 3 for clarity. Then,

$$\begin{aligned} C_{\theta i} &= \frac{P_i - P_7}{P_i - \overline{P}} \qquad i = 1, 2, ..., 6 \\ C_\phi &= \frac{P_{cw} - P_{ccw}}{P_i - \overline{P}}, \end{aligned} \tag{4}$$

where $C_{\theta i}$ and $C_{\phi i}$ are sets of coefficients sensitive to θ and ϕ, respectively; P_{cw} and P_{ccw} are the pressures recorded at the holes located adjacent to the ith hole in the clockwise and counter-

clockwise directions, respectively, and $\overline{P}$ (the approximation of the static pressure) must be redefined as $\overline{P} = (P_{cw} + P_{ccw})/2$. The static and stagnation pressure coefficients may then be defined as

$$\begin{aligned} C_0 &= \frac{P_i - P_0}{P_i - \overline{P}} \\ C_s &= \frac{\overline{P} - P_s}{P_i - \overline{P}}, \end{aligned} \tag{5}$$

where it has been recognized that for large flow angles, P_i (as the maximum pressure recorded on the probe tip) provides the best approximation of P_0. The functional dependence of the coefficients C_α and C_β (or, equivalently, $C_{\theta i}$ and $C_{\phi i}$), C_0 and C_s upon α and β (or θ and ϕ) may then be determined by calibration. Seven sets of discrete (but presumably piecewise-continuous) calibration functions will result; the appropriate calibration functions are selected depending on which hole i registers the highest pressure.

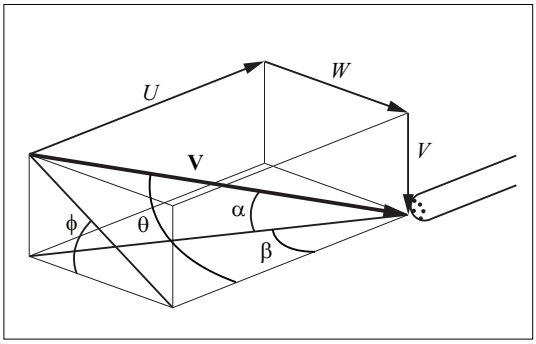

Figure 3. Graphical representation of velocities in pitch/yaw and spherical coordinate systems.

When subjected to an unknown velocity, the hole registering the maximum pressure is identified and the appropriate coefficients are evaluated from either (1) or (4). The flow angularity is determined from the corresponding calibration function, together with the corresponding values of C_0 and C_s. The individual velocity components may then be resolved, as

$$\begin{aligned} U &= |\mathbf{V}|\cos(\alpha)\cos(\beta) &&= |\mathbf{V}|\cos(\theta) \\ V &= |\mathbf{V}|\sin(\alpha) &&= |\mathbf{V}|\sin(\theta)\sin(\phi) \\ W &= |\mathbf{V}|\cos(\alpha)\sin(\beta) &&= |\mathbf{V}|\sin(\theta)\cos(\phi). \end{aligned} \tag{6}$$

The velocity magnitude $|\mathbf{V}|$ is obtained from (3) or (5) and the Bernoulli equation, as

$$|\mathbf{V}| = \left(\frac{2\Delta P}{\rho}\left(C_s - C_0 + 1\right)\right)^{1/2}, \tag{7}$$

where ΔP is the difference between the approximations of the stagnation and total pressures (in this case, $\Delta P = P_i - \overline{P}$), and ρ is the fluid density [10].

B. Generalized, n-hole probe calibration algorithm

Consider now a probe with a tip of arbitrary geometry, having n holes. As was the case for the conventional seven-hole probe, the local stagnation pressure may be approximated as the maximum pressure P_{max} recorded from the n holes. However, because the tip geometry and hole arrangement is arbitrary, no combination of holes can be identified *a priori* from which to obtain an average measure of the local static pressure. Instead, the closest available measure of static pressure is the minimum pressure P_{min} recorded from the n holes.

Using P_{min} and P_{max} as defined above, pressure coefficients may then be defined, as

$$\begin{aligned} C_j &= \frac{P_{max} - P_j}{P_{max} - P_{min}} \qquad j = 1, 2, ..., n \\ C_0 &= \frac{P_{max} - P_0}{P_{max} - P_{min}} \\ C_s &= \frac{P_{min} - P_s}{P_{max} - P_{min}} \end{aligned} \tag{8}$$

where P_j is the pressure recorded at the jth hole, and P_0 and P_s are again the reference total and static pressures, respectively. Note that $C_j = 0$ identically for the hole registering the largest pressure. These definitions are based upon the same reasoning used to obtain (1) and (3): that the error in the approximations of local stagnation and static pressure will become velocity-independent when normalized against the approximation of local dynamic pressure.

The pressure coefficients defined above have the advantages of being continuous throughout the range of calibration, and of being independent of the hole arrangement and the probe tip geometry. However, they are consequently more susceptible to error arising from flow separation (and therefore loss of accuracy in flows of high angularity); furthermore, if either P_{min} or P_{max} is recorded in a region of separated flow, this approach will necessarily fail.

With the pressure coefficients defined as shown in (8), a set of calibration data may be collected by recording the values of these coefficients with the probe oriented at a range of angles in α and β (or, equally, θ and ϕ) in constant, uniform flow at a single velocity. Assuming that all of the coefficients C_j are mutually independent, then α, β, P_0 and P_s will each be continuously and uniquely defined within the n-dimensional parameter space, so that

$$\begin{aligned} \alpha &= f_\alpha(C_1, C_2, ..., C_n) \\ \beta &= f_\beta(C_1, C_2, ..., C_n) \\ C_0 &= f_0(C_1, C_2, ..., C_n) \\ C_s &= f_s(C_1, C_2, ..., C_n) \end{aligned} \tag{9}$$

where f_α, f_β, f_0 and f_s are empirical functions defined by the calibration data. If the probe is then subjected to an unknown flow, the coefficients $(C_1, C_2, ..., C_n)$ obtained in that flow will describe a unique location within the n-dimensional hypercube. The flow angularity, C_0 and C_s (and thereby $|\mathbf{V}|$) may then be obtained by evaluating the functions f_α, f_β, f_0 and f_s at that point. This may be accomplished in the same way as is done for five- and seven-hole probes, using either look-up tables or curve fitting. The Cartesian velocity components may then be resolved in the same way as in the conventional seven-hole probe calibration procedure using (6) with $\Delta P = P_{max} - P_{min}$.

Alternatively, it is possible to approximate f_α, f_β, f_0 and f_s as continuous functions over the entire domain by fitting to polynomials of order k having n variables. However, previous work [22] has suggested that a polynomial of at least $k = 6$ is required. Then, if $n = 19$ (for example), this results in 177,100 terms, and the inversion of the calibration polynomial matrix becomes computationally intractable.

For the purposes of this work, the coefficients were in all cases obtained from the calibration data using third-order interpolation (see, for example, [8, 9]). Formally, then, f_α, f_β, f_0 and f_s were approximated as piecewise bicubics.

C. Extension of generalized calibration scheme to high-speed flows

The generalized n-hole probe calibration scheme described above requires that the fluid density remain constant; consequently, it is necessarily limited to flows of low Mach numbers. However, when multi-hole probes are used in high-speed flows, the directionality of the flow is obtained in much the same way as it is in low-speed flows.

Conventionally, the nondimensional coefficients C_α and C_β (or C_θ and C_ϕ) are defined using the same pressure differences as in (1), except that the pressures are normalized against the upstream dynamic pressure (which needs to be determined separately, and may require iteration) [23]. Because the generalized calibration scheme described above operates on nondimensional coefficients sensitive only to flow angularity, it may equally be used to resolve the directionality of high-speed flows using an n-hole probe with an appropriate tip geometry.

D. Analytically-derived calibration function for the nineteen-hole probe

For the particular case of a probe with a hemispherical tip, the probe geometry is such that analytical relationships between the hole pressure and local flow velocity may be obtained [14, 24, 25]; in this way, the probe may be used without requiring empirical calibration. In all cases, however, the analytical calibration of probes requires some idealization of the probe tip geometry. Because the probe performance tends to be highly sensitive to the tip geometry, the small imperfections which are unavoidable in the manufacture of any probe contribute significantly to measurement error and generally preclude the use of analytically-derived calibration functions (especially at higher Reynolds numbers). On the other hand, for the case of probes having a large number of holes, the

impact of error arising from imperfections affecting only some small number of the holes will be reduced as a consequence of the high level of data redundancy. The use of analytically-derived calibration functions for the nineteen-hole probe was therefore investigated.

The flow around the probe tip is assumed to approximate potential flow around a sphere, so that the local surface pressure (normalized by the far-field dynamic pressure) varies linearly with the square of the cosine of the relative flow cone angle, such that

$$\frac{2}{\rho\left|\mathbf{V}\right|^2}\left(P - P_s\right) = \frac{9}{4}\cos^2(\theta') - \frac{5}{4}, \tag{10}$$

where P is the surface pressure at some point p on the sphere, and θ' is the angle subtended between the incident velocity vector and the position vector of p (relative to an origin at the centre of the sphere). If the cone and roll angles describing the position vector of p on the surface of the probe tip are θ_p and ϕ_p, respectively, then

$$\begin{aligned}\cos(\theta') \;=\; & \sin(\theta)\cos(\phi)\sin(\theta_p)\cos(\phi_p) \\ & + \sin(\theta)\sin(\phi)\sin(\theta_p)\sin(\phi_p) \\ & + \cos(\theta)\cos(\theta_p).\end{aligned} \tag{11}$$

Substituting (11) into (10) will then yield a single equation relating the pressure at p to the magnitude and direction of the velocity incident upon the sphere. Given a hemispherical-tip probe having n pressure ports, the pressures $P_1, P_2, ..., P_n$ are known; equally, since the probe tip geometry is fixed, the locations of each hole $\theta_p = \theta_1, \theta_2, ..., \theta_n$ and $\phi_p = \phi_1, \phi_2, ..., \phi_n$ are also known. Then, (10) yields a system of n equations in θ, ϕ and $|\mathbf{V}|$. If $n = 3$, the system may be solved exactly; however, for cases of $n \geq 4$, more robust estimates of θ, ϕ and $|\mathbf{V}|$ may be obtained by treating the system as an unconstrained optimization problem. In this case, (10) may be alternatively expressed as a set of n equations,

$$\frac{2}{\rho\left|\mathbf{V}\right|^2}\left(P_j - P_s\right) - \frac{9}{4}\cos^2(\theta'_j) + \frac{5}{4} = \epsilon_j \qquad j = 1, 2, ..., n, \tag{12}$$

where ϵ_j is a measure of the error at each hole. The total error ϵ_0 may be defined such that

$$\epsilon_0^2 = \sum_{j=1}^{n} \epsilon_j^2. \tag{13}$$

The system of equations given by (12) may then be solved, subject to the minimization of (13). For the purposes of the present work, a generic search function is used to determine θ, ϕ and $|\mathbf{V}|$ to within a resolution of at least 0.1%.

Because this data reduction procedure is sensitive to the probe tip geometry, and because the

probe tip geometry is likely to be subject to some manufacturing errors, the sensitivity of the probe response to errors in hole position has been assessed for the case of the 19-hole probe. A synthetic data set $P_1, P_2, ..., P_{19}$ was generated using (10), assuming a uniform flow field having $U = V = 0$. A random error of up to δ in hole position (including an error in local R) was then applied to the known hole locations, and the resultant velocity components were obtained by minimizing (13) and applying (6). Any measured cross-flow velocity magnitude $V_{xy} = (V^2 + W^2)^{1/2}$ is therefore an artifact of the data reduction process and is indicative of the resultant error. This process was repeated until the mean error achieved statistical convergence. Figure 4 shows V_{xy}/U_∞ as a function of δ/R. The error increases almost linearly with the error in tip geometry, with $V_{xy}/U_\infty \sim 40\delta/R$. These results suggest that the analytical calibration of the nineteen-hole probe was sufficiently robust that even large tolerances in the probe tip geometry will still result in an acceptable error magnitude.

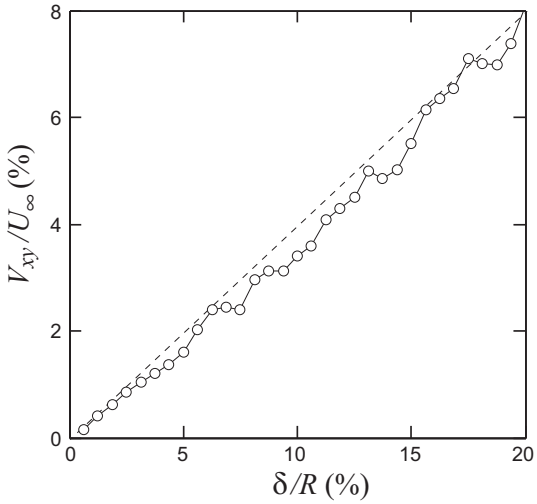

Figure 4. Error in cross-flow velocity magnitude as a function of error in hole position. ∘, computed values of V_{xy}/U_∞; - - -, $40\delta/R$

IV. Results

A. Validation of generalized calibration algorithm

In order to assess the effectiveness of the generalized calibration process, a single calibration data set was collected with the seven-hole probe, and the probe was then used to carry out a wake survey behind the wing model set at an angle of attack of 12°. Trailing vortex flows are fundamentally three-dimensional, and are characterized by both angularity and shear. These flows therefore provide a good test-case for the assessment of velocity probes.

Wake scan data were processed using both the conventional, sector-based seven-hole probe algorithm (1) - (5) and the new generalized algorithm (9). The normalized streamwise vortic-

ity $\zeta c/U_\infty$ was computed from the cross-flow velocity field using local bicubic fitting, and the resulting isovorticity contours are plotted in Figure 5. The maximum self-normalized vorticity $\zeta r_c/v_0$ (where r_c is the core radius and v_0 is the peak tangential velocity) was 2.626 and 2.484 for the conventional and generalized calibration techniques, respectively. However, the conventional, sector-based calibration technique resolved a secondary structure which was not apparent when the generalized calibration technique was used (Figure 5 a).

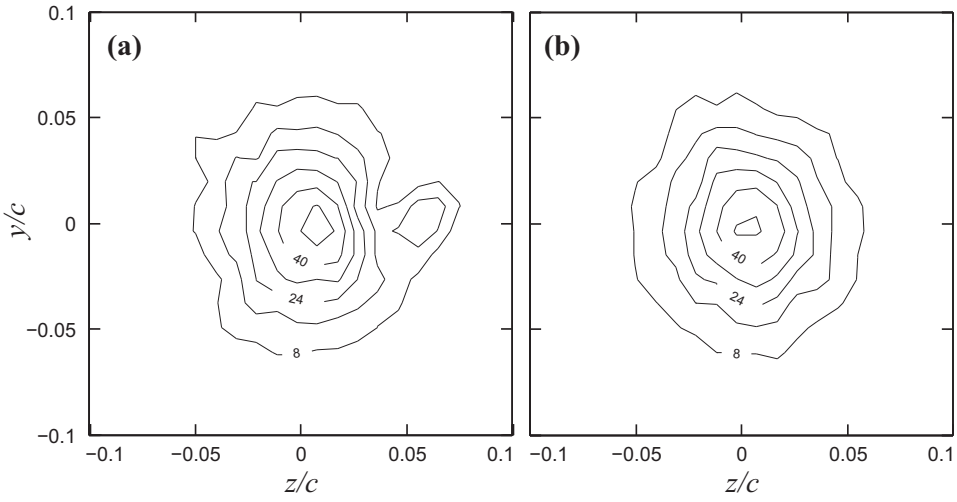

Figure 5. Contours of normalized vorticity $\zeta c/U_\infty$ from seven-hole probe measurements behind the wing at 12° incidence, using (a) conventional sector-based calibration technique, and (b) generalized calibration technique.

Since secondary structures are not typically expected to persist in wing wake surveys as far downstream as $x/c = 5$, the existence of a pronounced secondary vortex in the wake was investigated further. Figure 6 (a) shows isocontours of the pressure coefficient $C_{P7} = 2P_7/\rho U_\infty^2$ from the central hole of the seven-hole probe. The contours are skewed toward the positive-z axis, suggesting either a manufacturing defect in the probe tip or an initial misalignment between the probe axis and the tunnel axis. However, there are no localized disturbances in the pressure fields at the location of the secondary structure. The pressure fields from the six peripheral holes (not shown) likewise do not demonstrate any localized irregularities. Since concentrations of vorticity are normally associated with local pressure defects, these results appear to be contradictory.

Figure 6 (b) shows the isovorticity contours obtained using the conventional seven-hole probe calibration algorithm (as in Figure 5 b) together with the spatial regions in which the discrete calibration function for each hole i was used. From this plot, it is apparent that the secondary structure occurs directly upon the interface of two calibration sectors. Since there is no evidence of the existence of a secondary structure in the direct pressure measurements, it may be concluded that the secondary structure was an artifact of the conventional calibration scheme. Since secondary structures within regions of high vorticity can be common in wake surveys [21], the use of discrete calibration functions may yield misleading results.

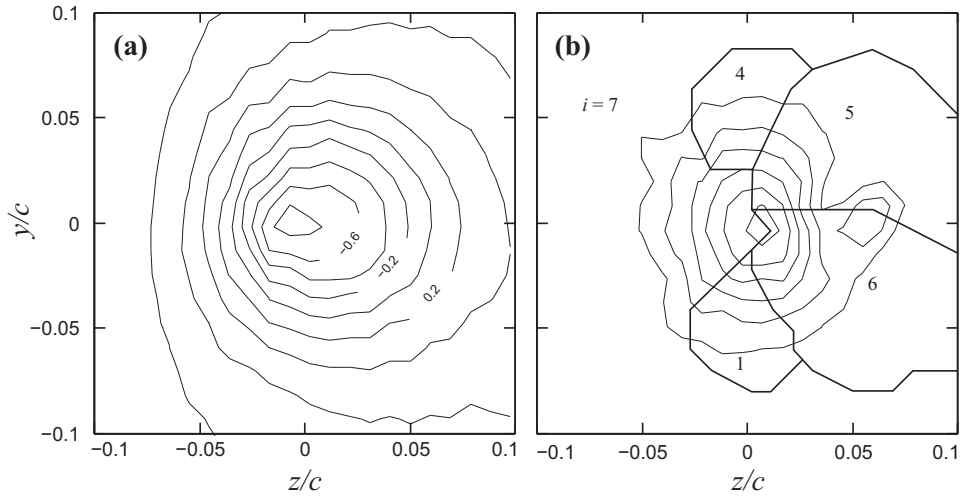

Figure 6. (a) Contours of C_P from the central hole of the seven-hole probe; (b) Contours of $\zeta c/U_\infty$ for the case of the conventional seven-hole probe calibration, showing the use of individual sectors.

B. Validation of nineteen-hole probe using generalized calibration

Because probes with hemispherical tip geometries have characteristically low ranges of sensitivity, the response of the nineteen-hole probe to flows of high angularity was assessed directly and compared to that of the conical seven-hole probe. The probes were first calibrated, and then positioned at a series of prescribed angles (α, β) in steady flow at constant U_∞. The flow angles returned by the probes (using the generalized calibration and data reduction scheme) were then compared to the prescribed angles. The nineteen-hole probe was accurate to within a mean error of 0.5° over the range $-60^\circ \leq \alpha \leq 60^\circ$ and $-60^\circ \leq \beta \leq 60^\circ$, compared to a mean error of 1.2° for the seven-hole probe (Figure 7). The nineteen-hole probe also demonstrated a much higher level of accuracy at large angularity. Note that the calibration remained monotonic within this range of flow angles, and so did not appear to be affected by any flow separation on the probe tip.

The relative accuracy of the probes is quantitatively demonstrated in Figure 8 (a), which shows the mean error in flow angularity $\overline{\Delta(\alpha,\beta)}$ as a function of the prescribed flow cone angle θ_0, where

$$\Delta(\alpha,\beta) = \left((\alpha-\alpha_0)^2 + (\beta-\beta_0)^2\right)^{1/2}, \tag{14}$$

and α_0 and β_0 are the prescribed pitch and yaw angles, respectively. The plot shows results from the seven-hole and nineteen-hole probes, both using the generalized calibration scheme within an angular range of $-60^\circ \leq \alpha \leq 60^\circ$ and $-60^\circ \leq \beta \leq 60^\circ$. Note that results are also shown for the analytically-calibrated nineteen-hole probe, though over a reduced range of $-30^\circ \leq \alpha \leq 30^\circ$ and $-30^\circ \leq \beta \leq 30^\circ$. Throughout the range of angles, the calibrated nineteen-hole probe provides an error of less than 0.75°, and provides typical improvement in accuracy of $\sim 0.25^\circ$ over the seven hole probe. Figure 8 (b) shows the probability distributions of $\Delta(\alpha,\beta)$ for the same data. The

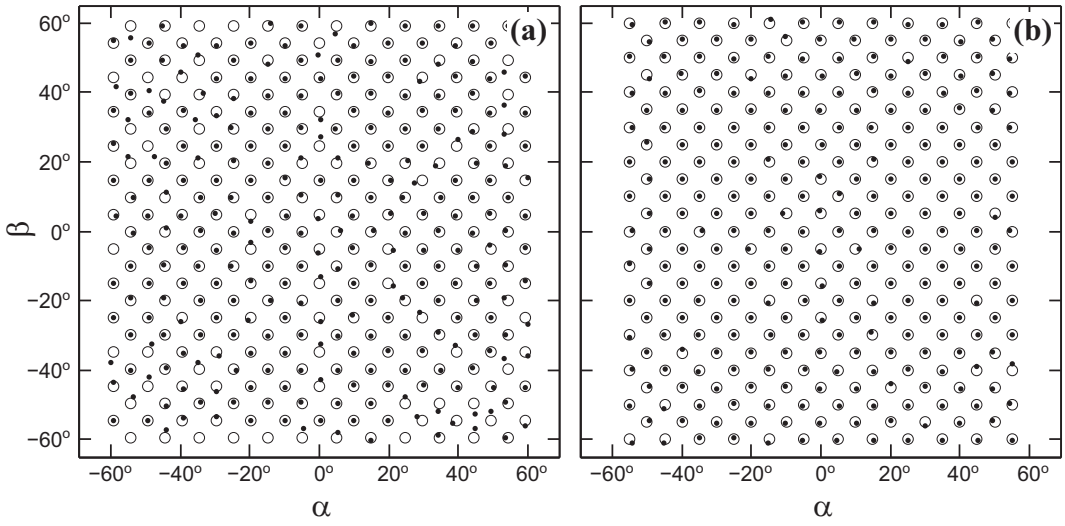

Figure 7. Demonstration of the angular range of the (a) seven-hole probe, and (b) nineteen-hole probe, both using the generalized calibration scheme. ○, prescribed angle; ●, measured angle.

calibrated nineteen-hole probe has both a narrower distribution and a substantially reduced tail relative to the seven-hole probe.

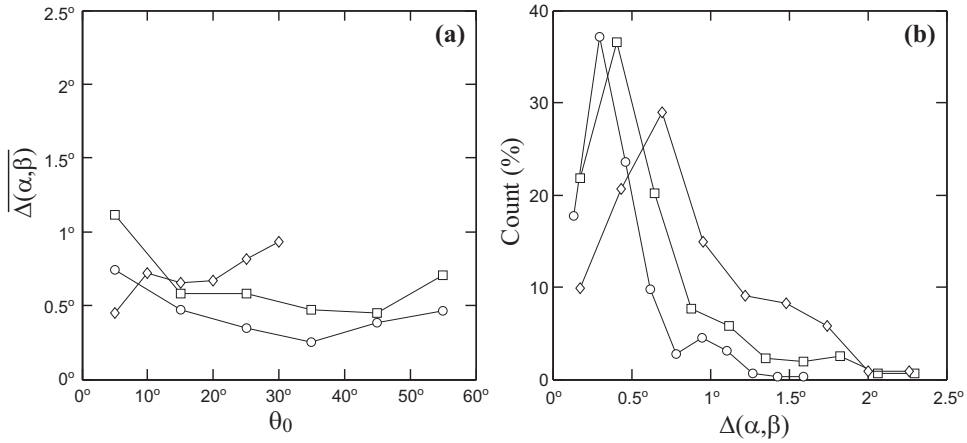

Figure 8. Distributions of error in flow angularity. (a) Mean error as a function of cone angle; (b) error probability density functions. □, seven-hole probe using generalized calibration scheme; ○, nineteen-hole probe using generalized calibration scheme; ◇, nineteen-hole probe using analytical calibration.

Both the seven-hole probe and the nineteen-hole probe were then used to obtain wake survey data behind the wing, set at a 5° angle of attack. The cross-flow velocity vectors, streamwise vorticity fields and streamwise velocity fields obtained with the two probe systems are compared in Figure 9. As expected, the results are almost indistinguishable. The nineteen hole probe does, however, appear to have slightly better resolved the velocity and vorticity at the centre of the vortex, likely as a consequence of its higher sensitivity to flow angularity.

The tip vortex formed downstream of a finite wing is expected to agree well with the ax-

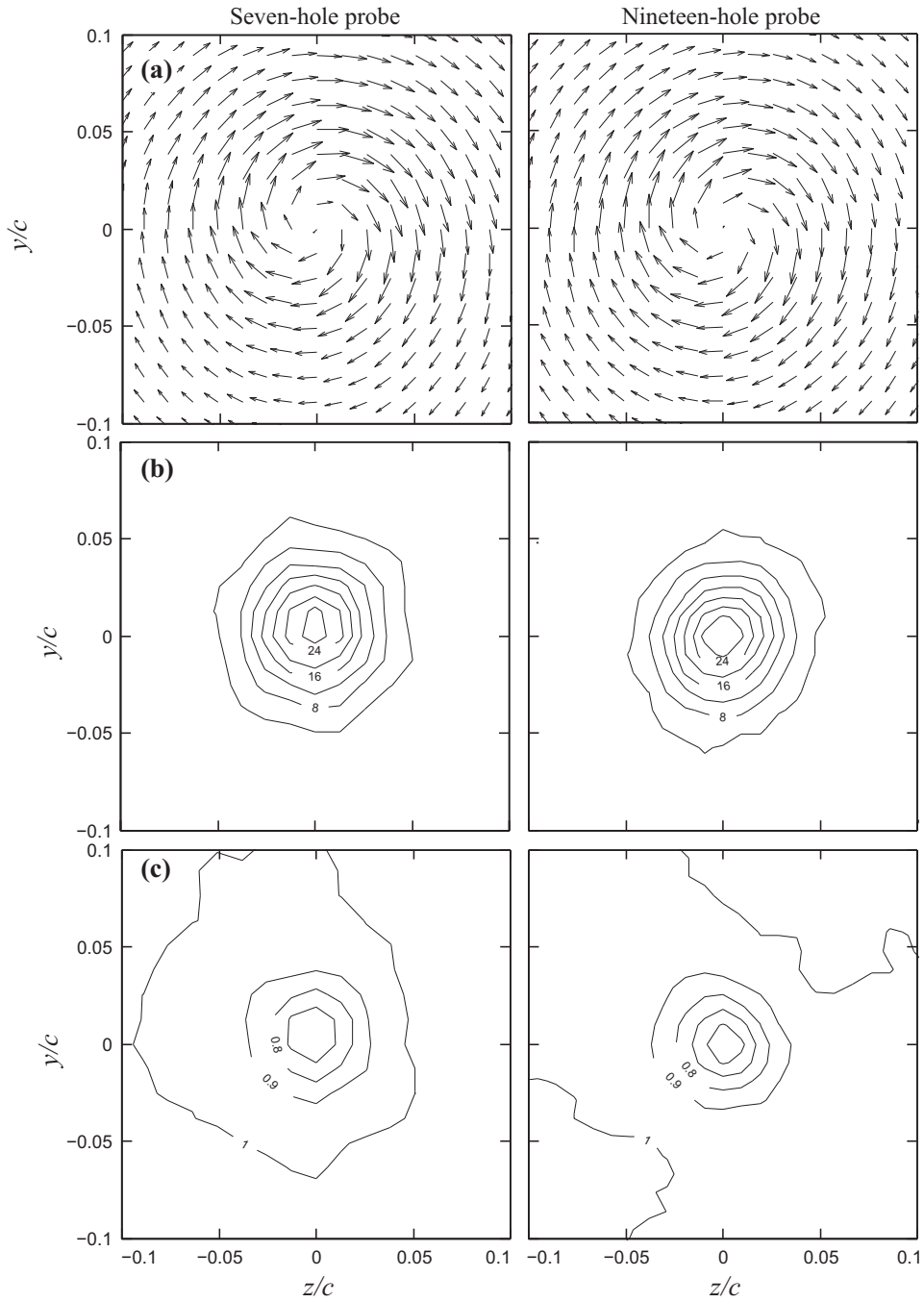

Figure 9. (a) Cross-flow velocity vector fields, and contours of (b) $\zeta c/U_\infty$ and (c) U/U_∞ for the seven-hole probe (left) and nineteen hole probe (right).

isymmetric Batchelor [19] profile, through a wide range of experimental parameters [20]. Radial profiles of self-scaled circulation $\Gamma(r)/\Gamma_c$ (where r is the radial coordinate relative to the vortex centre, and Γ_c is the circulation at $r = r_c$) were computed from the vorticity fields measured with

both probe systems, and the results were compared to the self-similar Batchelor solution,

$$\frac{\Gamma(r)}{\Gamma_c} = \frac{1 - \exp\left(-ar^2/r_c^2\right)}{1 - \exp(-a)}, \tag{15}$$

where $a \approx 1.25643$ is Lamb's constant. The circulation profiles obtained with both probe systems agree very well with (15) for $0 \lesssim r/r_c \lesssim 1.5$.

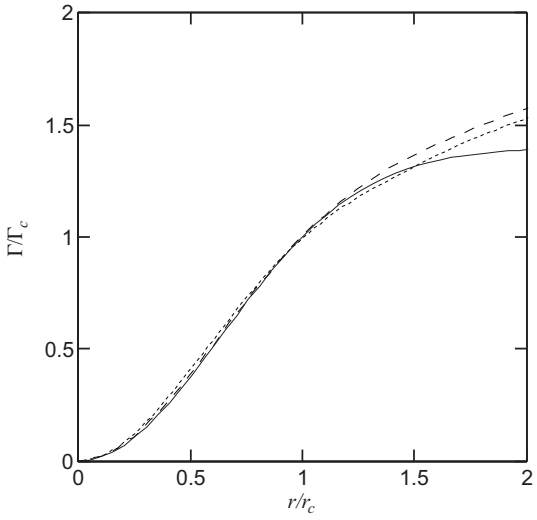

Figure 10. Core-normalized radial circulation profiles. – – –, Seven-hole probe; - - -, nineteen-hole probe; ——, (15).

C. Data redundancy and robustness of generalized calibration scheme

In order for a pressure-based velocity probe to adequately resolve the velocity components in three-dimensional flow, at least four mutually independent pressure signals from the probe tip are required. For probes having $n > 4$, then, a generalized calibration scheme (which is independent of the probe tip geometry) would enable the probe to function should one or more of the pressure signals be deemed unusable in post-processing.

To test the robustness of the calibration scheme described by (9), the pressure signals collected by the nineteen-hole probe during the wake survey shown in Figure 9 were re-processed using only data from some number k of randomly-selected holes (where $k = 4, 5, ..., n-1$). A cross-flow velocity error field $\epsilon(k)$ was defined, as

$$\epsilon(k) = \frac{\left|(V_k^2 + W_k^2)^{1/2} - (V_n^2 + W_n^2)^{1/2}\right|}{(V_n^2 + W_n^2)^{1/2}} \tag{16}$$

(where the subscripts k and n indicate the number of holes used to obtain the corresponding estimates of V and W). This estimate of error has the advantage of being a scalar quantity sensitive

to differences in both the direction and magnitude of the velocity vector. The mean error $\bar{\epsilon}$ was then computed as a spatial average over the cross-flow field (which had a maximum flow angularity of $\pm\sim 25^\circ$). This process was repeated, eliminating different randomly-selected holes, until $\bar{\epsilon}$ achieved statistical convergence. The variation of $\bar{\epsilon}$ with k is plotted in Figure 11, which also shows the extrema obtained for individual combinations of holes removed. For $k > 12$, the error was always less than $\sim 1\%$. However, for $k \leq 8$, the mean error in the cross-flow velocity fields remained within $\sim 1\%$, while the maximum error was within $\sim 3\%$. Measurements of the velocity components are therefore possible using the nineteen-hole probe and the current calibration technique with as many as any eleven of the individual sensors inoperative.

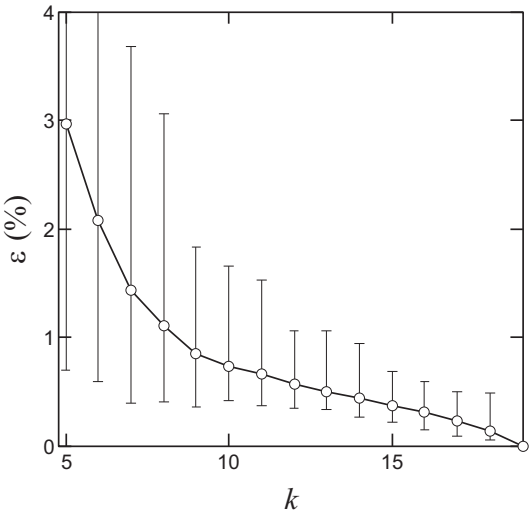

Figure 11. Variation in the mean cross-flow velocity error parameter $\bar{\epsilon}$. Error bars indicate range of values obtained.

D. Assessment of the analytical calibration scheme with the nineteen-hole probe

In order to assess the the validity of the analytical calibration scheme described in Section D, data was collected with the probe positioned at a range of prescribed angles (α, β) in a uniform free-stream flow. Although this technique derives from the assumption of inviscid flow and therefore low Reynolds numbers $Re_D = U_\infty D/\nu$ (where D is the diameter of the probe tip), Pisasale & Ahmed [25] show that flows of angularity of less than 60° may be resolved for $Re_D \lesssim 1600$. In the present work, $Re_D \sim 3300$, so care was taken in the validation and assessment of the the range of sensitivity.

The response of the probe is plotted in Figure 12, which shows the prescribed pitch and yaw angles, together with the corresponding pitch and yaw angles obtained from the data reduction algorithm. For angles within $\pm\sim 15^\circ$, the error in flow angularity is within the range of measurement uncertainty. For flow angles up to $\pm\sim 30^\circ$, the error in pitch and yaw increases to as much as 2.5°. The error distributions within this range of flow angles are also shown quantitatively in

Figure 8, together with the calibrated seven-hole and nineteen-hole probe results for comparison. Surprisingly, at flow angles of $\theta < 10°$, the analytically calibrated probe was more accurate than the experimentally calibrated one, though the mean error increases rapidly with increasing θ above $10°$, and the distribution of error is broad.

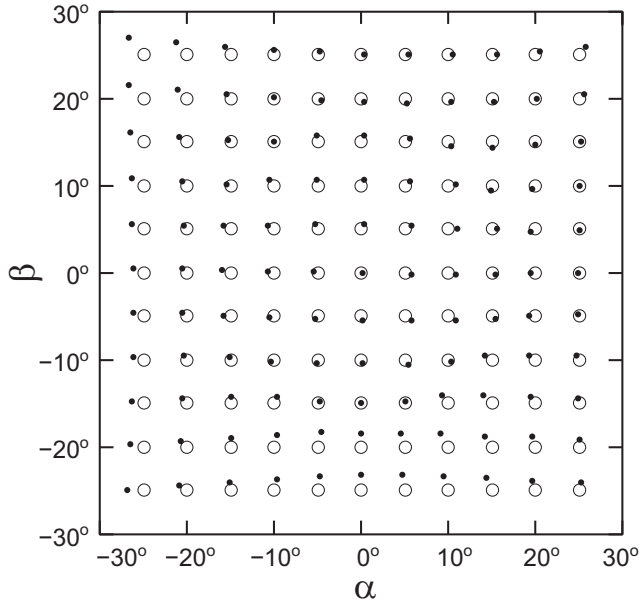

Figure 12. Demonstration of the angular range of the analytical calibration. ○, prescribed angle; ●, measured angle.

The nineteen-hole probe may therefore be expected to provide good accuracy, providing that measurements are made in flow fields having small angularity ($\lesssim \pm 15°$ in pitch and yaw). Since the calibrated post-processing of the wake survey data from the wing at $5°$ incidence (see Figure 9) showed regions with flow angularities both within and outside of this range, these data were used to assess the use of the analytically-calibrated nineteen-hole probe in a vortical flow field.

Figure 13 shows contours of $\zeta c/U_\infty$ and U/U_∞ for the analytically-calibrated nineteen-hole probe; these are directly comparable to the data shown in Figures 9 (b) and (c). These results are almost indistinguishable from the results obtained using the calibrated probes; the contours are nearly circular, and the maximum and minimum values are within the range of experimental uncertainty.

E. Direct measurement of local velocity gradients using generalized calibration

Intrusive probes are occasionally used for the direct measurement of local velocity gradients, either using multiple hot-wire elements [26] or pressure taps [27]. Typically, these probes provide independent measures of velocity at several locations in space, separated by distances with length-scales of the order of those of the probe measurement volume. By assuming that the velocity is constant within the probe volume (which is equivalent to the assumption that $(R/U_\infty)dV_i/dx_j$ is

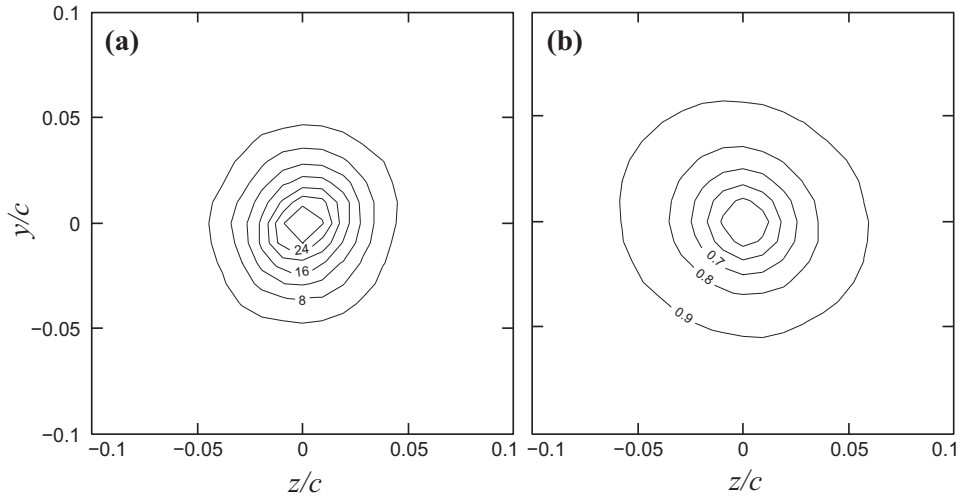

Figure 13. Contours of (a) $\zeta c/U_\infty$ and (b) W/U_∞, obtained behind the wing set at 5° incidence using the analytically-calibrated nineteen-hole probe.

negligible), mean velocity gradients within the volume may be obtained. While estimates of local velocity gradients may always be obtained from wake survey data by computing the gradients of the velocity fields, these estimates will be subject to increased error owing to the sensitivity of the gradients to small errors in the measurement locations. Also, computing spatial gradients from a wake survey grid requires the assumption that $(\Delta x/U_\infty)dV_i/dx_j$ is negligible (where Δx is the spatial resolution of the measurement grid). Consequently, for flows with high, local concentrations of vorticity (such as wing wakes), local measurements of the gradients are preferable.

Because the nineteen-hole probe is able to obtain velocity measurements always accurate to within $\sim 2\%$ with as many as ten arbitrarily selected pressure signals discarded (for flows of angularity of at least $\pm 25^\circ$; see Figure 11), it is possible to obtain multiple, independent local measures of velocity by separately processing data from subsets of the nineteen holes. As an extension, if the holes in the probe head are assigned to four overlapping quadrants (as shown in Figure 14), quasi-independent measurements of the velocity components will be available at the approximate spatial locations $(x, y \pm R/4, z \pm R/4)$, where (x, y, z) is the nominal measurement point. Since both V and W will be independently available from two different known locations in y and two different known locations in z within the same cross-flow plane, it is possible to obtain local estimates of the cross-flow velocity gradients.

Figure 15 shows isocontours of the normalized velocity gradients $(c/U_\infty)dV/dy$ and $(c/U_\infty)dW/dz$ obtained from the single-point nineteen-hole probe measurements (left) and from conventional field estimates (right); these are the same data as presented in Figure 9. Significant differences between the two gradient estimates are observed. The local measurements have a vanishing value near the origin, and lobes of positive and negative values in each of the four quadrants (though the estimate of dV/dy was corrupted by some bad vectors in the $z > 0$, $y < 0$

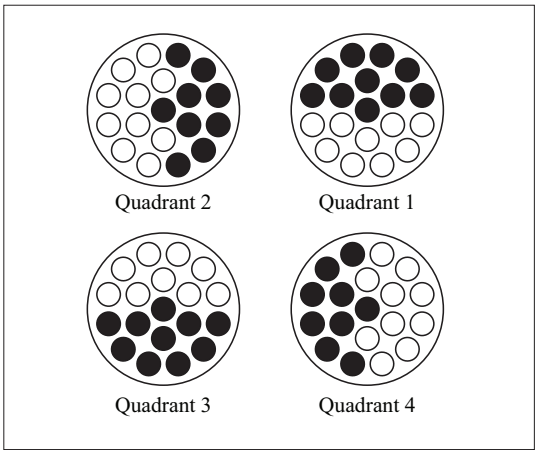

Figure 14. Holes used to obtain spatially-separated measurements of velocity.

quadrant), while the field estimates have a local maximum near the origin.

These results may be compared to the gradients of an axisymmetric Batchelor vortex,

$$\frac{dW}{dz} = -\frac{dV}{dy} = \frac{2V_0}{r_c^3}\left(1+\frac{1}{2a}\right)\frac{yz}{\eta^4}\left[1-\left(a\eta^2+1\right)\exp\left(-a\eta^2\right)\right], \tag{17}$$

(where $\eta = r/r_c$) which has extreme values of $dW/dz = \pm 0.5242 V_0/r_c$ at $z = \pm y = 0.8448 r_c$, and vanishes along the y and z axes. For the data shown, (17) predicts local extrema of $(c/U_\infty)dW/dz = \pm 5.29$ at $y/c = \pm z/c \sim 0.028$. The large, nonzero values of the gradients obtained at the vortex centre by field estimates is therefore likely to be an artifact of the poor spatial resolution of the scan relative to the scale of the vortex core (for the data shown in Figure 15, $r_c/\Delta x \sim 3$). The peak magnitudes of the gradients and the spatial locations of these peaks were similar for both the local measurements and the field estimates; these also agreed with those predicted by (17).

The velocity gradients dW/dy and dV/dz could not be obtained reliably from the test-case velocity field using this technique. The distribution of the gradients obtained were subject to a high degree of noise and distortion. This poor agreement is likely due to the magnitude of the gradient. For the case of a Batchelor vortex,

$$\frac{dW}{dy} = \frac{2V_0}{r_c^3}\left(1+\frac{1}{2a}\right)\frac{y^2}{\eta^4}\left[1-\left(a\eta^2+1\right)\exp\left(-a\eta^2\right)-\frac{r_c^2}{2y^2}\eta^2\left(1-\exp\left(-a\eta^2\right)\right)\right], \tag{18}$$

which has an extreme value of $dW/dy = 1.7564 V_0/r_c$ at the origin (note that $dV/dz = -dW/dy$ when subjected to a 90° rotation). The peak absolute magnitude of $(c/U_\infty)dW/dy$ expected was therefore ~ 18, corresponding to $(R/U_\infty)dW/dy \sim 0.37$, which is not negligible. This large gradient is likely to have resulted in significant error due to probe interference effects [28, 29], especially since the sampling holes have been clustered together (rather than being randomly distributed). However, the results presented in Figure 11 suggest that a probe of this design may be

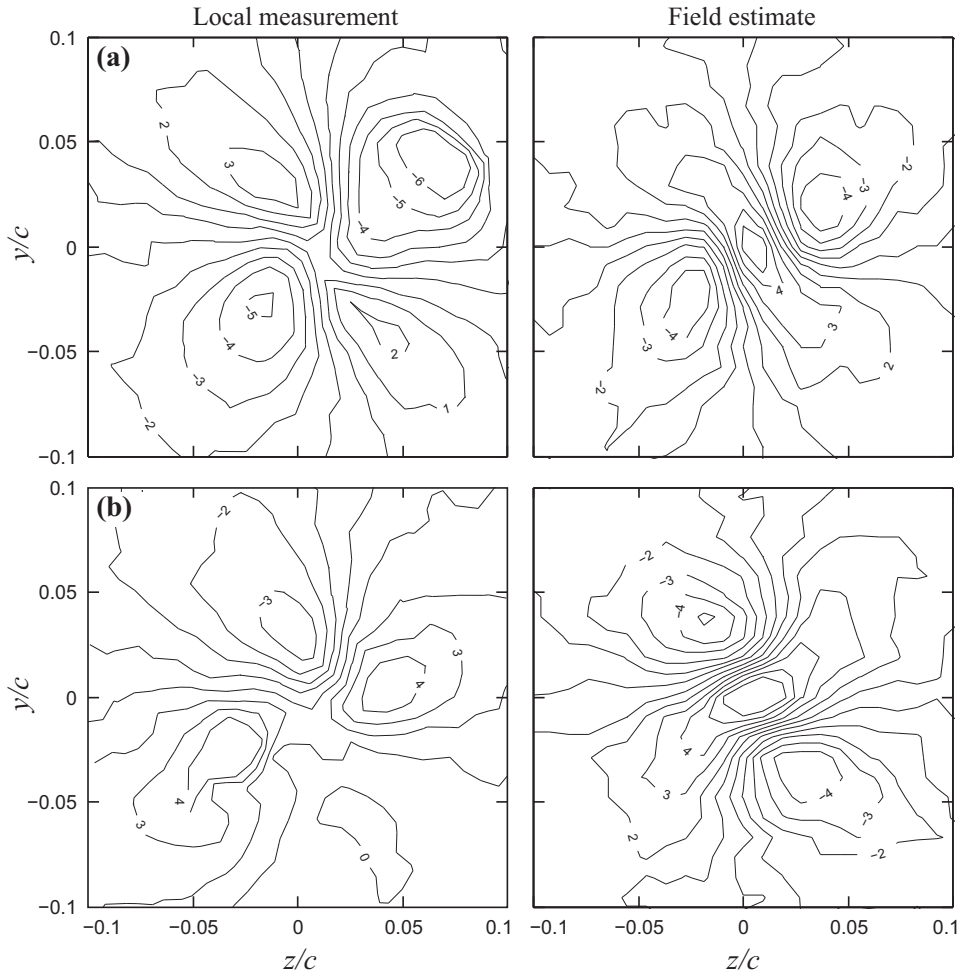

Figure 15. Contours of normalized velocity gradients in a vortex flow. (a) $(c/U_\infty)dU/dx$**, (b)** $(c/U_\infty)dV/dy$**; left, local measurements from nineteen-hole probe; right, field estimates.**

used to measure dW/dy and dV/dz in flows with smaller gradients.

V. Conclusions

The use of a miniature, nineteen-hole pressure probe and a generalized calibration algorithm in low-Re wing wake surveys is demonstrated. The calibration algorithm is particularly useful, since it is independent of the probe geometry and the number of active pressure taps, and therefore tolerant of data corruption and imperfections in probe manufacture.

The nineteen-hole probe was tested in the vortex wake behind a wing, as this flow offers a well-characterized and strongly three-dimensional velocity field with high angularity and shear. The nineteen-hole probe was able to accurately return the three components of velocity in the vortex wake, and yielded vorticity fields which were more closely axisymmetric than those obtained with a conventional seven-hole probe. The large number and high concentration of holes in the nineteen-hole probe, together with an n-dimensional calibration function, results in velocity mea-

surements which are less susceptible to error resulting from high velocity gradients or calibration data interpolation.

The large number of holes also allows the more accurate use of the probe with an analytical calibration function for flows with angularity of less than $\sim 15^\circ$, though this process necessarily requires a nominally hemispherical probe tip geometry. The sensitivity to error in probe tip geometry has been quantified, demonstrating that a mean error of as much as $0.1R$ in hole position will result in a measurement error of only $\sim 3\%$.

Quasi-independent velocity estimates were obtained from different subsets of holes in the nineteen-hole probe tip, in order to obtain local estimates of the cross-flow velocity gradients in a vortex wake. The diagonal components of the gradient tensor were accurately reproduced, and agreed well with the distribution characteristic of axisymmetric vortex flows. By comparison, finite-difference field estimates of the vorticity exhibited a high degree of error near the vortex centre, owing to the high vorticity and low spatial resolution of the wake scan. The off-diagonal components of the gradient tensor could not be obtained using the nineteen-hole probe, as the error sensitivity was too high in the vortex flow field.

Acknowledgments

This work was supported in part by the UK Engineering and Physical Sciences Research Council under grant number EP/H030360/1. The authors are very grateful to Dr. Paul Nathan for his assistance in the fabrication and integration of the instrumentation systems used.

References

[1] Maskell, E. C., "Progress towards a method for the measurement of the components of the drag of a wing of finite span," *Royal Aircraft Establishment Technical Report*, Vol. 72232, 1973.

[2] Kuzunose, K., "Drag prediction based on a wake integral method," *AIAA Paper*, Vol. AIAA-98-2723, 1998, pp. 501–514.

[3] Birch, D. M. and Lee, T., "Investigation of the near-field tip vortex behind an oscillating wing," *J. Fluid Mech.*, Vol. 544, 2005, pp. 201–241.

[4] Spalart, P., "On the far wake and induced drag of aircraft," *Journal of Fluid Mechanics*, Vol. 603, 2008, pp. 413–430.

[5] Lorber, P., McCormick, D., Anderson, T., Wake, B., MacMartin, D., M. Pollack, M., Corke, T., and Breuer, K., "Rotorcraft retreating blade stall control," *AIAA Paper*, , No. 2000-2475, 2000.

[6] Birch, D. M. and Martin, N., "Tracer particle momentum effects in vortex flows," *Journal of Fluid Mechanics*, Vol. 723, 2013, pp. 665–691.

[7] Treaster, A. L. and Yocum, A. M., "The calibration and application of five-hole probes," *ISA Transactions*, Vol. 18, No. 3, 1979, pp. 23–34.

[8] Gallington, R. W., "Measurement of very large flow angles with non-nulling seven-hole probes," *USAFA Aeronautics Digest*, Vol. USAFA-TR-80-17, 1980, pp. 60–88.

[9] Everett, K. N., Gerner, A. A., and Durston, D. A., "Seven-hole cone probes for high angle flow measurements: theory and calibration," *AIAA Journal*, Vol. 21, No. 7, 1996, pp. 992–998.

[10] Zilliac, G. G., "Calibration of seven-hole pressure probes for use in fluid flows with large angularity," *NASA Technical Memorandum*, , No. 102200, 1989.

[11] Tropea, C., Yarin, A., and Foss, J., *Springer Handbook of Experimental Fluid Mechanics*, Springer, 2007.

[12] Wenger, C. W. and Devenport, W. J., "Seven-hole pressure probe calibration method utilizing look-up error tables," *AIAA Journal*, Vol. 37, No. 6, 1999, pp. 675–679.

[13] Sumner, D., "A comparison of data-reduction methods for a seven-hole probe," *Journal of Fluids Engineering*, Vol. 124, 2002, pp. 523–527.

[14] Kjelgaard, S. O., "Theoretical derivation and calibration technique of a hemispherical-tipped, five-hole probe," *NASA Technical Memorandum*, , No. 4047, 1988.

[15] Ramakrishnan, V. and Rediniotis, O. K., "Calibration and data-reduction algorithms for nonconventional multihole pressure probes," *AIAA Journal*, Vol. 43, No. 5, 2005, pp. 941–952.

[16] Ramakrishnan, V. and Rediniotis, O. K., "Development of a 12-hole omnidirectional flow-velocity measurement probe," *AIAA Journal*, Vol. 45, No. 6, 2007, pp. 1430–1432.

[17] Wang, H., Chen, X., and Zhao, W., "Development of a 17-hole omnidirectional pressure probe," *AIAA Journal*, Vol. 50, No. 6, 2012, pp. 1426–1429.

[18] Benay, R., "A global method of data reduction applied to seven-hole probes," *Experiments in fluids*, Vol. 54, 2013, pp. 1535.

[19] Batchelor, G. K., "Axial flow in trailing line vortices," *Journal of Fluid Mechanics*, Vol. 20, 1964, pp. 645–658.

[20] Birch, D. M., "Self-similarity of trailing vortices," *Physics of Fluids*, Vol. 24, No. 2, 2012, pp. 1–16.

[21] Birch, D. M., Lee, T., Mokhtarian, F., and Kafyeke, F., "Structure and induced drag of a tip vortex," *J. Aircraft*, Vol. 41, No. 5, 2004, pp. 1138–1145.

[22] McParlin, S. C., Ward, S. S., and Birch, D. M., "Optimal calibration of directional velocity probes," *51st AIAA Aerospace Sciences Meeting, Grapevine, TX, January 2013*, 2013, pp. AIAA 2013–0045.

[23] Cantolanzi, F. J., "Characteristics of a 40° cone for measuring Mach number, total pressure and flow angles at supersonic speeds," Tech. Rep. NACA-TN-3967, National Advisory Committee for Aeronautics, 1957.

[24] Pisasale, A. J. and Ahmed, N. A., "Theoretical calibration for highly three-dimensional low-speed flows of a five-hole probe," *Measurement Science and Technology*, Vol. 13, No. 7, 2002, pp. 1100–1107.

[25] Pisasale, A. J. and Ahmed, N. A., "Development of a functional relationship between port pressures and flow properties for the calirbation and application of multihole probes to highly three-dimensional flows," *Experiments in Fluids*, Vol. 36, 2004, pp. 422–436.

[26] Vukoslavcevic, P. V., Beratlis, N., Balaras, E., Wallace, J. M., and Sun, O., "On the spatial resolution of velocity and velocity gradient-based turbulence statistics measured with multi-sensor hot-wire probes," *Physics of Fluids*, Vol. 46, No. 1, 2009, pp. 109–119.

[27] Freestone, M. M., "Vorticity measurement by a pressure probe," *Aeronautical Journal*, Vol. 92, 1988, pp. 29–35.

[28] Lighthill, M. J., "Contributions to the theory of the Pitot tube displacement effect," *Journal of Fluid Mechanics*, Vol. 2, No. 5, 1957, pp. 493–512.

[29] Cousins, R. R., "A note on shear flow past a sphere," *Journal of fluid mechanics*, Vol. 40, No. 3, 1970, pp. 543–547.